Exploring the Feasibility of Differentiating IEEE 802.15.4 Networks to Support Health-Care Systems

Youn-Soon Shin, Kang-Woo Lee, and Jong-Suk Ahn

Abstract: **IEEE 802.15.4 networks are a feasible platform candidate for connecting all health-care-related equipment dispersed across a hospital room to collect critical time-sensitive data about patient health state, such as the heart rate and blood pressure. To meet the quality of service requirements of health-care systems, this paper proposes a multi-priority queue system that differentiates between various types of frames. The effect of the proposed system on the average delay and throughput is explored herein. By employing different contention window parameters, as in IEEE 802.11e, this multi-queue system prioritizes frames on the basis of priority classes. Performance under both saturated and unsaturated traffic conditions was evaluated using a novel analytical model that comprehensively integrates two legacy models for 802.15.4 and 802.11e. To improve the accuracy, our model also accommodates the transmission retries and deferment algorithms that significantly affect the performance of IEEE 802.15.4. The multi-queue scheme is predicted to separate the average delay and throughput of two different classes by up to 48.4% and 46%, respectively, without wasting bandwidth. These outcomes imply that the multi-queue system should be employed in health-care systems for prompt allocation of synchronous channels and faster delivery of urgent information. The simulation results validate these model's predictions with a maximum deviation of 7.6%.**

Index Terms: **Analytical model, health-care systems, IEEE 802.15.4, multiple queues, quality of service (QoS) service.**

I. INTRODUCTION

To provide ubiquitous health-care services such as distant diagnosis and remote operations regardless of location and time, hospitals have recently begun to integrate health-care-related devices in hospital rooms into small-scale networks and then connect them to the Internet. For scalability purposes, these health-care networks tend to be organized into a two-tier hierarchy [1]–[5]—backbone and access networks—each of which is configured to efficiently perform different tasks. At the bottom level, various wireless sensor networks are deployed to continuously accumulate patient health information, such as the blood pressure, heart rate, pulse, and body temperature, even when the patient is on the move without encumbering the patient with wires. At the upper tier, which provides access to the Internet, various types of networks are placed with the aim of rapid transfer of data gathered from their lower networks to distantly located high-speed servers while sporadically directing commands in the opposite direction. Typical examples of core networks are IEEE 802.3 [6] or IEEE 802.11 [7] networks, whereas IEEE 802.15.4 [8], [9] and IEEE 802.15.1 [10] networks are examples of lower ones.

Since health-care systems require timely and reliably transfer of patient sensing data from their edge networks, an IEEE 802.15.4 networking is an especially feasible platform candidate for an access network to collect health-related data due to its low cost, limited energy consumption, and QoS support. Note that the IEEE 802.15.4 protocol is a representative medium access control (MAC) protocol suitable for low-rate wireless personal area networks (LR-WPAN). These desirable features of IEEE 802.15.4 allow as many as 128 nodes in a single cell to effectively communicate for a long time without any interruptions caused by battery changes as long as the amount of traffic to deliver is acceptable.

However, since the IEEE 802.15.4 standard only supports a transfer rate of up to 250 kbps, it cannot provide sufficient bandwidth for the various health-care applications that dump a large amount of data during a short interval. We believe that the applicability of IEEE 802.15.4 is limited to applications in which nodes sense and report physiological data such as electrocardiography (EKG), electroencephalography (EEG), pulse oximeter data, blood pressure, and cardiac output—applications whose data generation rates are known to be less than 100 kbps according to [5].

To minimize energy waste and provide synchronous transmission, IEEE 802.15.4 structures its transmission time into superframes, where the boundary is signaled by special frames named beacons that are periodically broadcast by the coordinator. A superframe is divided into sleep and active periods whose durations can be dynamically readjusted whenever beacons are delivered. Furthermore, the active period is split into two adjustable intervals, contention access period (CAP) and contention free period (CFP), which are designated to carry asynchronous and synchronous traffic, respectively. In CAP, nodes need to contend with each other to send their data, while in CFP, a node should reserve one synchronous channel a priori. Once one channel is assigned in CFP, the node is guaranteed to constantly send data that are regularly estimated, such as the heart rate and pulse of patients

However, IEEE 802.15.4 lacks some mechanisms essential for it to be adopted as an access network for health-care systems. To be precise, it has no mechanism to differentiate between ordinary frames and urgent ones commanding the swift reservation of CFP synchronous channels during emergencies and the reconfiguration of a sensor's functionality. For example, when the

Manuscript received September 30, 2010.

This research was supported by the basic science research program through the National Research Foundation (NRF) of Korea funded by the Ministry of Education, Science and Technology (2010-0013237).

Y.-S. Shin and K.-W. Lee are with the Information Communication Engineering Department, University of Dongguk, 26, Pil-dong 3-ga, Jung-gu, Seoul, Korea, email: {ysshin, klee}@dgu.edu.

J.-S. Ahn is with the Computer Engineering Department, University of Dongguk, 26, Pil-dong 3-ga, Jung-gu, Seoul, Korea, email: jahn@dgu.edu.

1229-2370/11/$10.00 © 2011 KICS

heart beats abnormally, a doctor may want to see more detailed information pertaining to the heart by activating additional attached sensors which would usually be turned off to reduce both data traffic and transmission power.

In other words, IEEE 802.15.4 cannot prioritize important frames such as guaranteed time slot (GTS) requests and crucial frames over common data frames in CAP during which each node runs the carrier sensing multiple access (CSMA)/collision avoidance (CA) algorithm to fairly deliver frames, therefore possibly incurring frequent collisions. Note that to reserve a synchronous channel in CFP, nodes should transmit a GTS request frame during the previous CAP.

To effectively satisfy these QoS demands of health-care systems, this paper proposes to equip multiple transmission queues into nodes of IEEE 802.15.4 as in IEEE 802.11e [11], which maintains four transport queues to handle different traffic classes based on their level of urgency. The multi-queue system can distinguish time-critical frames from time-insensitive ones by granting different transmission priorities. Here, each queue is implemented by assigning different contention window operational parameters. To explore the impacts of this multi-queue system in terms of the average delay and throughput under both saturated and unsaturated conditions, this paper also introduces an analytical model that comprehensively combines two performance models for IEEE 802.15.4 [12]–[21] and IEEE 802.11e [22].

Our model differs from the previous model [23] in three points as follows. First, our model faithfully abstracts the multi-queue system, where each node runs a scheduler resolving virtual collisions among its multiple queues. In contrast, since the previous model has no such scheduler, it can only evaluate networks where each node holds one different priority queue. Second, it greatly improves the accuracy of the delay and throughput model by including two significant mechanisms of IEEE 802.15.4, namely, the maximum retries and deferment techniques, which are explained in Section III. Finally, it completes the delay model to estimate the average time taken to build a new synchronous channel and the appropriate timeout for applications to wait to recover abandoned frames by IEEE 802.15.4.

Our analytical model evaluation clarified that the multi-queue scheme can sufficiently separate the delay and throughput of multiple different priority classes by varying a few parameters determining the contention window size. For instance, with two classes, it predicts that the higher class surpasses the lower one by up to 48.4% and 46% in terms of average delay and throughput, respectively, without deteriorating overall utilization. This means that the multi-queue system can quicken the synchronous channel allocation by 52.8% compared to the traditional single-queue system. In terms of the influence of the deferment scheme, the average delay was shown to grow by up to 10.7% as the CAP interval shrinks. Simulation results verified our mathematical model's accuracy for the average delay and throughput analysis to a maximum discrepancy of 7.6%.

This paper is organized as follows. Section II describes the multi-queue system implementation in IEEE 802.15.4, and Section III explains its mathematical model. Section IV compares predictions from the analytical model with results from simulations. Finally, Section V summarizes conclusions and future research.

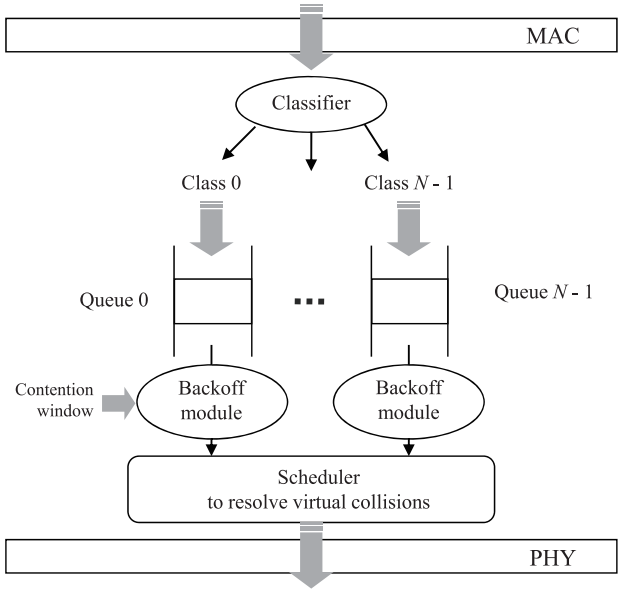

Fig. 1. Interior view for the multi-queue system of a node.

II. MULTIPLE TRANSMISSION QUEUES IN IEEE 802.15.4

Fig. 1 illustrates the block diagram of our IEEE 802.15.4 multi-queue scheme in a node for prioritizing traffic. It is comprised of two components: A classifier distributing frames to their appropriate queues among N available queues according to their types and a scheduler deciding their transmission order. In this paper, we assume that higher class numbers correspond to higher priorities.

Whenever a new frame arrives from the upper layer, the classifier chooses one of the queues to store it depending on its type. Once the newly arrived frame is buffered, the classifier executes the associated backoff module to randomly pick its backoff delay from the contention window. Note that for the newly arrived frame, the CA algorithm determines the contention window. After that, the binary exponential backoff (BEB) algorithm doubles the contention window at each transmission failure. In this scheme, each queue's transmission priority is distinguished by associating two different contention window parameters, namely, macMinBE, and macMaxBE, which decide the minimum and maximum, respectively, of the window's upper bound.

After a frame's transmission is either successfully or unsuccessfully finished, the transmission scheduler is invoked to find the next frame with the smallest backoff delay from the multiple queues. When the backoff delays of two or more different priority queues are the same, it resolves this virtual collision by offering the channel access right to the frame in the higher priority queue. For other frames with equal backoff delay, the scheduler calls their corresponding backoff module to recalculate their new backoff delay since they are considered to virtually collide.

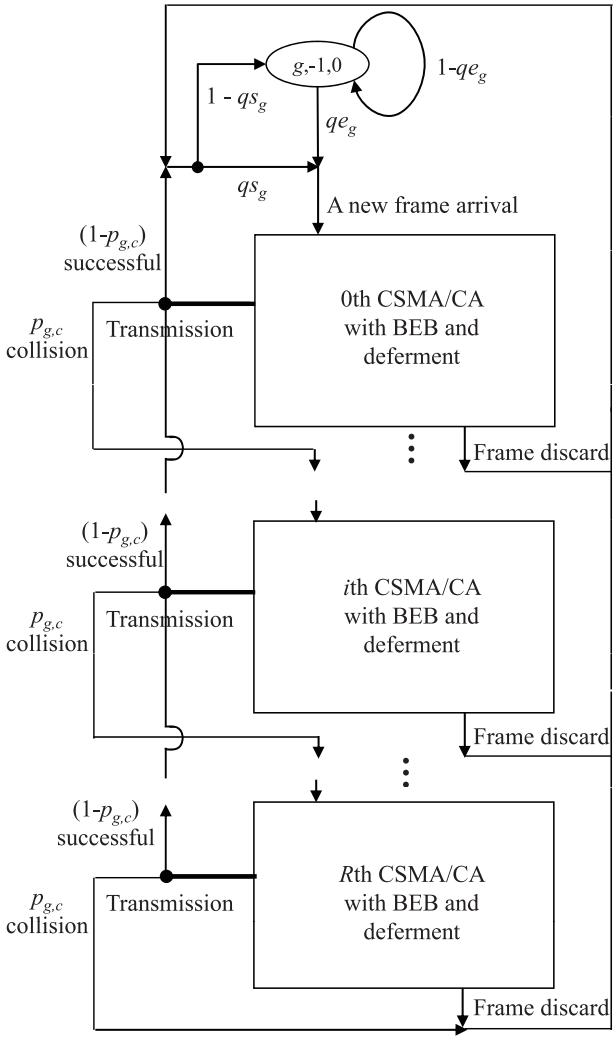

Fig. 2. Block diagram of IEEE 802.15.4 Markov chain with transmission retries.

III. ANALYTICAL PERFORMANCE MODEL OF THE MULTI-QUEUE SYSTEM

A. Extended Model of IEEE 802.15.4 with Deferment and Transmission Retries Algorithm

Fig. 2 describes a complete Markov chain block diagram abstracting the behavior of IEEE 802.15.4 running on class g ($g = 0, \cdots, N-1$) with transmission retries that specifies that a frame should be abandoned after a predetermined maximum number of retransmissions. In Fig. 2, a frame of class g is dropped after $(R+1)$th collisions. After a frame of class g is generated with probability qe_g from the idle state $(g, -1, 0)$, IEEE 802.15.4 tries to transmit the frame by feeding it into boxes labeled as 0th CSMA/CA with BEB and deferment algorithm, whose behaviors are elaborated in Fig. 3. Here, qe_g is the probability that at least one frame of class g is passed down from the upper layer during the average time slot, $E[\text{slot}]$. Since we assume that the traffic of class g is produced by the Poisson process with an average rate of λ_g, qe_g is calculated as $qe_g = 1 - e^{-\lambda_g E[\text{slot}]}$.

After ith CSMA/CA with BEB and deferment is executed in Fig. 2, there are three possible outcomes represented by three arrows from each box: Collision, successful transmission, and frame discard. For the first case, when a frame is decided to have crashed by the absence of its acknowledgement frame, IEEE 802.15.4 continues to go into the next subsequent box until it reaches the Rth box.

For the second case, it goes all the way up to the idle state to check if there are frames waiting at the class g queue. If there is already at least one new frame with probability qs_g, it will immediately run 0th box. Note that qs_g is just the probability that the class g output queue of a node is not empty. It is calculated by $E[DF_g]\lambda_g$, where λ_g represents the class g traffic generation rate while $E[DF_g]$ denotes the average service time per frame of class g. To evaluate the behavior of 802.15.4 networks when they become saturated, qs_g is grown up to 1 while $E[DF_g]$ is set to a constant. Otherwise, it stays at the idle state with probability $(1 - qe_g)$ until a new frame arrives. For the third case, it throws away the current frame and moves to the top to search a new frame, just like in the second case.

Fig. 3 presents a discrete Markov chain describing the detailed behavior of each small box labeled as ith CSMA/CS with BEB and deferment in Fig. 2. In Fig. 3(a), each circle represents a state of IEEE 802.15.4 with three state variables, g, j, and k, where g, j $(\in (0, M))$, and k $(\in (0, W_{g,j} - 1))$ are the class identification, number of backoffs that have elapsed, and current backoff counter, respectively. The state probability $b_{g,j,k}$ associated with each state is calculated as $b_{g,j,k} = \lim_{t\to\infty} P\{s(g,t) = j, w(g,t) = k\}$. This notation $b_{g,j,k}$ refers to the state (g, j, k) in the rest of the paper.

For the deferment scheme, Fig. 3(a) adds a small box labeled as Df on top of each $b_{g,j,0}$ state where IEEE 802.15.4 starts the deferment algorithm to determine whether it has enough time to send a frame in this CAP. The deferment technique stipulates that when a frame's transmission cannot be completed within a given CAP, the treatment of that frame should be postponed to the next CAP. If the remaining time is insufficient with probability p_d, it loops back to the current stage to pick up a new backoff delay when the subsequent CAP starts [13], [14]. The probability p_d is sought by $p_d = (2\text{CCA} + L_{\text{Frame}} + T_{\text{wACK}} + L_{\text{ACK}} + \text{IFS} - 1)/L_{\text{CAP}}$, where L_{Frame}, T_{wACK}, L_{ACK}, IFS, and L_{CAP} denote the transmission delay of one data frame, waiting time before the acknowledgement frame arrive, transmission delay of the acknowledgement frame, inter-frame space time, and length of contention access period, respectively. Fig. 3(b) unfolds this deferment state broken into Rt sub-states to account for the time elapsed before the next CAP begins. Note that Rt represents the average remaining time in time slots when a frame should be deferred.

When IEEE 802.15.4 has sufficient time, it runs the clear channel assessment (CCA) algorithm, which scans the channel twice to determine its availability. When the channel is detected to be occupied at either scan trial with probability α_g or β_g, it runs the BEB algorithm to multiplicatively expand the contention window. When both the deferment and first CCA test are passed as shown in Fig. 3(a), state $b_{g,j,0}$ transits to the next state $b_{g,j,-1}$ with probability $(1-p_d)(1-\alpha_g)$. After the second CCA succeeds, it can send the frame.

$$\tau_g = \sum_{i=0}^{R}(P_{g,c}(1-p^{M+1}))^i \sum_{j=0}^{M} b_{g,j,0}$$
$$= \begin{cases} \dfrac{1-(P_{g,c}(1-p_g^{M+1}))^{R+1}}{1-p_{g,c}(1-p_g^{M+1})} \Big/ \Big(\dfrac{(1-q_s)}{q_e} + L(1-p_d)(1-p_g^{M+1}) - \dfrac{1}{2}(1-q_e)p_d(W_{g,0}-1) \\ +\Big(\dfrac{3}{2} - \alpha_g - (1-\alpha_g - Rt)p_d\Big)\dfrac{1-p_g^{M+1}}{1-p_g} + \dfrac{W_{g,0}}{2}\dfrac{1-(2p_g)^{M+1}}{1-2p_g}\Big), & \text{when } M \le \mathrm{macMaxBE} - \mathrm{macMinBE} \\ \dfrac{1-(P_{g,c}(1-p_g^{M+1}))^{R+1}}{1-p_{g,c}(1-p_g^{M+1})} \Big/ \Big(\dfrac{(1-q_s)}{q_e} + L(1-p_d)(1-p_g^{M+1}) - \dfrac{1}{2}(1-q_e)p_d(W_{g,0}-1) \\ +\Big(\dfrac{3}{2} - \alpha_g - (1-\alpha_g - Rt)p_d\Big)\dfrac{1-p_g^{M+1}}{1-p_g} + \dfrac{W_{g,0}}{2}\dfrac{1-(2p_g)^{M_d+1}}{1-2p_g} + \dfrac{W_{g,0}2^{M_d}}{2}\dfrac{p_g^{M_d+1}(1-p_g^{M-M_d})}{1-p_g}\Big), \\ \qquad\qquad \text{when } M > \mathrm{macMaxBE} - \mathrm{macMinBE}. \end{cases} \tag{2}$$

To account for the average time consumed for a frame's transmission, Fig. 3(a) puts a box labeled with Tx in front of $b_{g,j,-1}$. Fig. 3(c) illustrates the magnified view of the Tx box containing L states, indicating that the average transmission time of a frame is L in the unit of the time slots.

$$\begin{cases} P\{b_{g,j,k}|b_{g,j,k+1}\} = 1, & j \in (0,M), k \in (0, W_{g,j}-2) \\ P\{b_{g,j,-1}|b_{g,j,0}\} = (1-\alpha_g)(1-p_d), & j \in (0,M) \\ P\{b_{g,j,k}|b_{g,j-1,0}\} = \dfrac{\alpha_g(1-P_d)}{W_{g,j}}, & j \in (1,M), k \in (0, W_{g,j}-1) \\ P\{b_{g,0,k}|b_{g,M,0}\} = \dfrac{\alpha_g(1-P_d)}{W_{g,0}}, & k \in (0, W_{g,0}-1) \\ P\{b_{g,j-2,L-1}|b_{g,j,-1}\} = 1-\beta_g, & j \in (0,M) \\ P\{b_{g,j,k}|b_{g,j-1,-1}\} = \dfrac{\beta_g}{W_{g,j}}, & j \in (1,M), k \in (0, W_{g,j}-1) \\ P\{b_{g,0,k}|b_{g,M,-1}\} = \dfrac{qs_g\beta_g}{W_g,0}, & k \in (0, W_{g,0}-1) \\ P\{b_{g,0,k}|b_{g,j,-2,0}\} = \dfrac{(1-p_{g,c})qs_g}{W_{g,0}}, & j \in (0,M), k \in (0, W_{g,0}-1) \\ P\{b_{g,-1,0}|b_{g,j,-2,0}\} = (1-p_{g,c})(1-qs_g), & j \in (0,M) \\ P\{b_{g,0,k}|b_{g,j,-2,0}\} = \dfrac{p_{g,c}}{W_{g,0}}, & j \in (1,M), k \in (0, W_{g,0}-1) \\ P\{b_{g,0,k}|b_{g,j,-2,0}\} = \dfrac{gs_g}{W_{g,0}}, & j \in (0,M) \\ P\{b_{g,-1,0}|b_{g,j,-2,0}\} = (1-qs_g), & j \in (0,M) \\ P\{b_{g,-1,0}|b_{g,-1,0}\} = 1-qe_g & \\ P\{b_{g,0,k}|b_{g,-1,0}\} = \dfrac{qe_g}{W_{g,0}}, & k \in (0, W_{g,0}-1). \end{cases} \tag{1}$$

Equation (1) evaluates all state transition probabilities $P\{b_{g,j,k}|b_{g',j',k'}\}$ from state $b_{g,j,k}$ to state $b_{g',j',k'}$ in Fig. 3(a) in terms of $\alpha_g, \beta_g, W_{g,j}, p_d, p_{g,c}, qe_g$, and qs_g, where $W_{g,j}$ is the maximum window size of class g at the jth backoff stage. Based on these transition probabilities in (1), (2) solves the probability τ_g that a given node attempts the first CCA. The calculation of τ_g branches into one of the two equations according to the value of M, which represents the maximum number of backoffs, namely macMaxCSMABackoffs. Note that M_d in the second equation of (2) is $\mathrm{macMaxBE}-\mathrm{macMinBE}$, where the two constants macMinBE, and macMaxBE denote the minimum and maximum exponent values defining the upper bound of the contention window. In (2), $p_g(=\alpha_g+(1-\alpha_g)\beta_g)$ is the probability of encountering the busy channel at either one of the two CCA scans.

Equations (3) and (4) express α_g and β_g with τ_g and n_g, where n_g is the total number of competing nodes with class g queues. Since the set of these equations is hard to solve analytically, all parameters such as α_g, β_g, and τ_g were numerically calculated in our experiments. Furthermore, note that these equations differ from the previous model [23] in that they include the modified factor $\prod_{h=0}^{g}(1-\tau_h)^{n_h-1}\prod_{h=g+1}^{N-1}(1-\tau_h)^{n_h}$ to accommodate the effect of the virtual collision resolver which excludes queues with lower priority than class g in the same node from competition over the underlying physical channel.

$$\alpha_g = \Big[L(1-\prod_{h=0}^{g}(1-\tau_h)^{n_h-1}\prod_{h=g+1}^{N-1}(1-\tau_h)^{n_h})\Big](1-\alpha_g)(1-\beta_g), \tag{3}$$

$$\beta_g = \frac{1-\prod_{h=0}^{g}(1-\tau_h)^{n_h-1}\prod_{h=g+1}^{N-1}(1-\tau_h)^{n_h}}{2-\prod_{h=0}^{N-1}(1-\tau_h)^{n_h}}. \tag{4}$$

B. Two Delay Models for 802.15.4 with Multi-Queue System

This section computes two average delays of the multi-queue system: The average frame delay and average service delay of class g as shown in (5) and (12), respectively.

First, the average frame delay $E[DF_g]$ in (5) is defined as the time taken for a node to transfer a given frame of class g before the next frame is sent. It is divided into two kinds of delays: The sum of $E[DCB_g]$ and $E[DST_g]$ for successful transmission, and the sum of $E[DCD_g]$ and $E[DBD_g]$ for unsuccess-

ful transmission due to transmission retries and channel capture failures.

$$E[DF_g]=E[DCB_g]+E[DST_g]+E[DBD_g]+E[DCD_g]. \quad (5)$$

In (6), $E[DCB_g]$ averages the time accumulating all backoff delays, while $E[DST_g]$ is divided into two average delay components: One for all failed transmissions due to collision and another for the final transmission and waiting time for the acknowledgement to return. Here, T_c, T_s, and $T_{\mathrm{macAckWaitDuration}}$ are the time that one collision consumes, the time spent for one successful transmission, and maximum timeout, respectively.

$$\begin{aligned}
E[DCB_g] &= \sum_{i=0}^{R}(p_{g,c}(1-p_g^{(M+1)}))^i(1-p_{g,c})E[D_{g,\mathrm{CSMA}}],\\
E[DST_g] &= T_c\sum_{i=0}^{R} i(p_{g,c}(1-p_g^{(M+1)}))^i(1-p_{g,c})+T_s p_{g,\mathrm{success}},\\
E[DBD_g] &= \sum_{i=0}^{R}(p_{g,c}(1-p_g^{(M+1)}))^i E[DD_g],\\
E[DCD_g] &= p_{g,\mathrm{discardcollision}}\sum_{i=0}^{R}E[D_{g,\mathrm{CSMA}}]+T_c(R+1)
\end{aligned} \quad (6)$$

where $T_c = (L_{\mathrm{Frame}} + T_{\mathrm{macAckWaitDuration}})\sigma$ and $T_s = (L_{\mathrm{Frame}} + T_{\mathrm{wACK}} + L_{\mathrm{ACK}} + \mathrm{IFS})\sigma$.

Equation (7) calculates $E[D_{g,\mathrm{CSMA}}]$ which is the sum of backoff delays that a frame undergoes from when it enters the small box shown in Fig. 3(a) until it leaves to be transmitted. In (7), the first two terms represent the backoff delays due to non-deferred and deferred operations, respectively, while the remaining term corresponds to the delay for CCA operations.

$$\begin{aligned}
E[D_{g,\mathrm{CSMA}}] &= E[X_g]\sigma + E[DX_g]\sigma\\
&\quad + (E[N_{g,\mathrm{CCAFail}}]E[N_{g,\mathrm{CCA}}]+2)T_{\mathrm{CCA}}.
\end{aligned} \quad (7)$$

In (7), $E[X_g]$, $E[DX_g]$, σ, and T_{CCA} are the average number of backoff slots when deferment does not occur, average number of waiting slots due to deferment, duration of one backoff slot, and duration of one CCA, respectively. $E[N_{g,\mathrm{CCAFail}}]$ and $E[N_{g,\mathrm{CCA}}]$ shown in (9) and (10) denote the average number of CCA failures due to the occupied channel and average number of CCA trials at a given backoff stage.

$E[X_g]$ and $E[DX_g]$ are calculated in (8), where $W_{g,j}$ is the number of time slots that a successfully transmitted frame consumes at the jth backoff stage, and $k_{g,j}$ is the probability that a node successfully sends a frame at the jth stage. Furthermore, L_{bcn} denotes the transmission delay of one beacon. In the third equation in (8) for $k_{g,j}, p_g^j(1-p_g)$ is the probability that a frame successfully departs for the link after reaching the jth backoff stage.

$$E[X_g] = \sum_{j=0}^{M} k_{g,j}E[W_{g,j}],$$

$$\begin{aligned}
&E[DX_g] = p_d(E[X_g] + \sum_{j=0}^{M} k_{g,j}(j+1)(Rt+L_{\mathrm{bcn}})),\\
&Rt = (2\mathrm{CCA} + L_{\mathrm{Frame}} + T_{\mathrm{wACK}} + L_{\mathrm{ACK}} + \mathrm{IFS} - 1)/2,\\
&k_{g,j} = p_g^j(1-p_g),\\
&E[W_{g,j}] = \sum_{h=0}^{j}(W_{g,h}-1)/2,
\end{aligned} \quad (8)$$

$$E[N_{g,\mathrm{CCAFail}}] = \sum_{j=0}^{M} jk_{g,j}, \quad (9)$$

$$E[N_{g,\mathrm{CCA}}] = 1 + (1-\alpha_g). \quad (10)$$

Equation (11) calculates $E[DD_g]$, the average time spent before discarding the frame due to another channel access failure after the Mth stage in Fig. 3.

$$\begin{aligned}
E[DD_g] = p^{(M+1)}\big(&\textstyle\sum_{j=0}^{M}\big(\frac{W_{g,j}-1}{2}+E[N_{g,\mathrm{CCA}}]\big)\\
&+p_d\big(\textstyle\sum_{j=0}^{M}\frac{W_{g,j}-1}{2}+(M+1)(Rt+L_{\mathrm{bcn}})\big)\big)\sigma.
\end{aligned} \quad (11)$$

Second, (12) calculates the average service delay $E[D_g]$ between two consecutive successful transmissions of class g.

$$E[D_g] = \sum_{j=0}^{\infty} p_{g,\mathrm{send}}(1-p_{g,\mathrm{send}})^j \sum_{k=0}^{j} E[DF_g]. \quad (12)$$

C. Probabilities of Frame Discards and Collisions

Equation (13) computes the probability of successful transmission $p_{g,\mathrm{send}}$ and two sorts of frame discard probabilities: $p_{g,\mathrm{discard\_collision}}$ and $p_{g,\mathrm{discard\_channelcapturefail}}$ due to the maximum transmission retries and maximum channel capture failures, respectively. Note that a frame is discarded only when the $(R+1)$th retransmission trial and $(M+1)$th channel capture fail.

$$\begin{aligned}
&p_{g,\mathrm{discard_collision}} = (p_{g,c}(1-p_g^{M+1}))^{R+1},\\
&p_{g,\mathrm{discard_channelcapturefail}} = (p_g^{M+1}\tfrac{1-(p_{g,c}(1-p_g^{M+1}))^{R+1}}{1-p_{g,c}(1-p_g^{M+1})},\\
&p_{g,\mathrm{send}}\\
&= 1-(p_{g,c}(1-p_g^{M+1}))^{R+1} - (p_g^{M+1}\tfrac{1-(p_{g,c}(1-p_g^{M+1}))^{R+1}}{1-p_{g,c}(1-p_g^{M+1})}.
\end{aligned} \quad (13)$$

Equation (14) calculates the collision probability $p_{g,c}$ that a frame of class g crashes. Note that a frame of class g experiences collision when any other node or any higher priority queue among classes from $(g+1)$ to $(N-1)$ in the same node sends frames in the same time slot. Note that the probabilities that all other nodes and higher priority queues in the same node do not capture the channel are $\prod_{h=0}^{N-1}(1-\tau_h)^{n_h-1}$ and $\prod_{h=g+1}^{N-1}(1-\tau_h)$, respectively.

$$\begin{aligned}
p_{g,c} &= 1-\prod_{h=0}^{N-1}(1-\tau_h)^{n_h-1}\prod_{h=g+1}^{N-1}(1-\tau_h)\\
&= 1-\prod_{h=0}^{g}(1-\tau_h)^{n_h-1}\prod_{h=g+1}^{N-1}(1-\tau_h)^{n_h}.
\end{aligned} \quad (14)$$

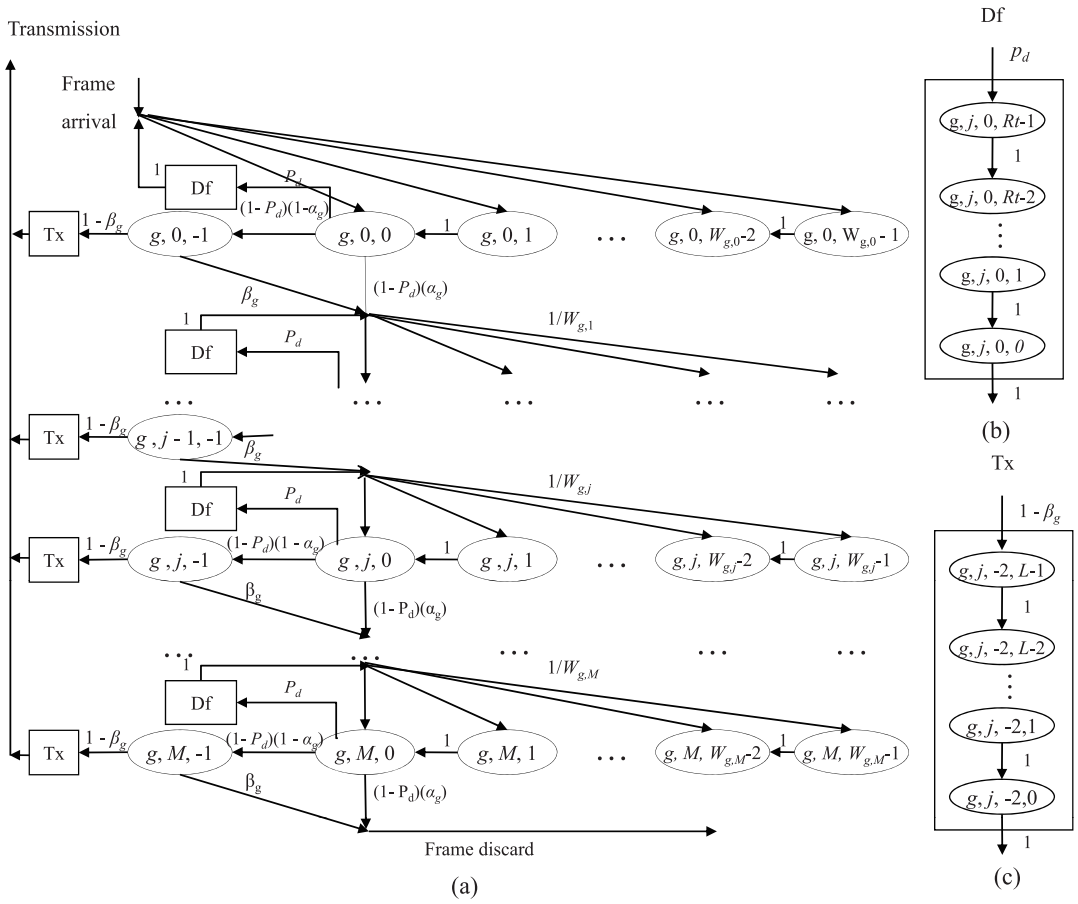

Fig. 3. Discrete Markov chain of IEEE 802.15.4 with deferment algorithm: (a) Total view of CSMA/CA with BEB and deferment, (b) inner view of deferment box, and (c) inner view of transmission box.

D. Throughput Model for 802.15.4 with Multiple Queues

The throughput of class g is evaluated by (15) in which throughput is defined as the fraction of the time that the channel is spent for successful transmission of frames in a unit time. In (15), $E[\text{slot}]$ is the average length of one slot time aUnitBackoffPeriod, and L_{payload} is the payload length in the number of slots.

$$S_g = \frac{p_{g,\text{success}} L_{\text{payload}}}{E[\text{slot}]}. \tag{15}$$

Equation (16) measures $p_{g,\text{success}}$, which is the probability that a frame of class g is transmitted successfully in one time slot.

$$p_{g,\text{success}} = n_g \tau_g \prod_{h=0}^{g} (1-\tau_h)^{n_h - 1} \cdot \prod_{h=g+1}^{N-1} (1-\tau_h)^{n_h} (1-\alpha_g)(1-\beta_g). \tag{16}$$

IV. EXPERIMENTS

This section evaluates the effect of the multi-queue system on the average frame delay, service delay, and throughput as a function of offered loads and number of classes by both our analytical models and simulations. For validation of our models, the results of the simulations were compared to those of the analytical models under both saturated and non-saturated situations. The simulation modules for the multi-queue system were implemented into ns-2 2.33 [24].

Table 1 summarizes the main operational parameters of IEEE 802.15.4 when the multi-queue system maintains three classes for a health-care system, e.g., the highest priority class for emergency data frames, the second-highest priority one for GTS request frames, and the lowest one for ordinary data frames. To distinguish these classes, we set three different parameters—macMinBE, macMaxBE, and macMaxCSMABackoffs—to differentiate the transmission priorities while sustaining default parameter values for other parameters over a 2.4 GHz channel.

Fig. 4 illustrates the effect of deferments on the average frame delay $E[DF_g]$ as computed by (5) when the number of nodes and superframe order (SO) vary. In Fig. 4, the curve of no-deferment is almost indistinguishably coincident with that of $\text{SO} = 9$. This is because the impact of deferments is quite negligible when the superframe lasts long enough to send many frames. However, the influence of deferments becomes apparent when SO becomes as small as 2 or 3, leading to a maximum 10.7% difference in frame delays from the model without deferments. This result shows that deferments heavily affect the av-

Table 1. System parameters.

Parameter	Value
Data frame payload	70 Bytes
GTS request frame payload	70 Bytes
PHY + MAC header	13 Bytes
ACK	11 Bytes
Channel Bit Rate	250 kbps
Duty cycle	100%
macMinBE	1–3
macMaxBE	5–8
macMaxCSMABackoffs	4–6
aMaxFrameRetries	3
SO	2, 3, 9

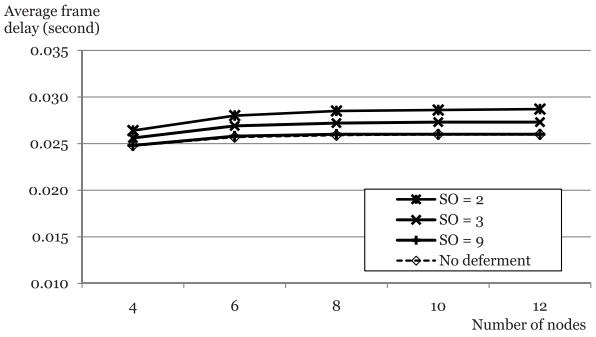

Fig. 4. Average frame delay variations due to deferments.

erage delay, especially when the superframe does not run long enough.

Fig. 5 shows the average service delay variations of each class in the multi-queue system computed by (12) as a function of the number of involved nodes. The offered load of each class was adjusted to be identical while macMaxBE for classes 0, 1, and 2 were set to 8, 6, and 5, respectively. Class 2 was confirmed to reduce the average service delay by around 52.8% at maximum. The expense for this better performance was only an 8% delay increase against class 0 compared to the delays of the single queue system when there are about six nodes.

However, for large numbers of nodes such as 12 or more, even class 0 exhibits a shorter average delay. This indicates that the multi-queue scheme improves its performance except when the network is lightly congested. Consequently, this result proves that our multiple queue system can tell apart service delays of different classes for enhancing QoS services without incurring much cost to the lowest priority class. Note that the Appendix presents more results for evaluating the effects of the three operational parameters on the service delays of the multi-queue system.

Fig. 6 plots the throughputs as a function of λ_g when five nodes with dual queues contend for the wireless channel. Class 1 outperforms class 0 under saturated conditions, while the throughputs of the two classes are mostly the same under unsaturated conditions. Fig. 6 also illustrates that the total throughput of the dual queue system is almost the same as that of the single-queue system, meaning that separation of the traffic classes does not hamper the overall performance. Finally, the throughput of

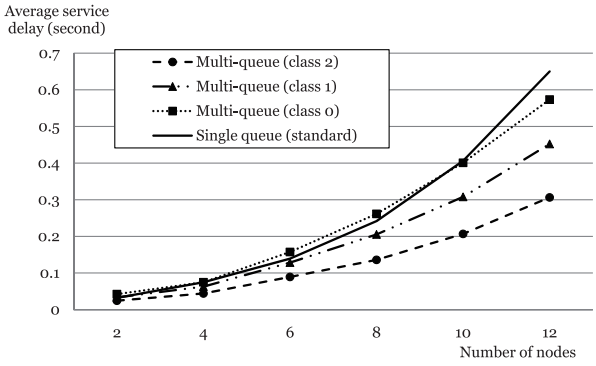

Fig. 5. Average service delay of single and multi-queue system.

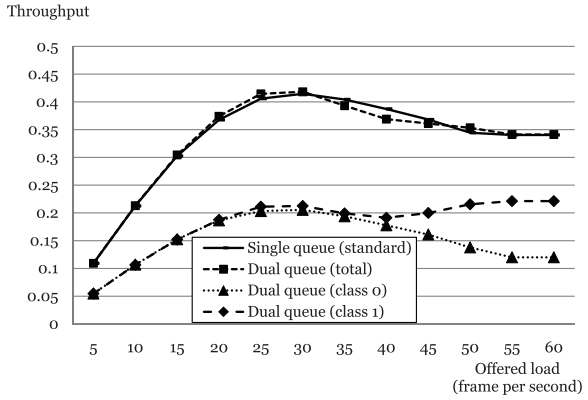

Fig. 6. Throughput variations of single and multi-queue system.

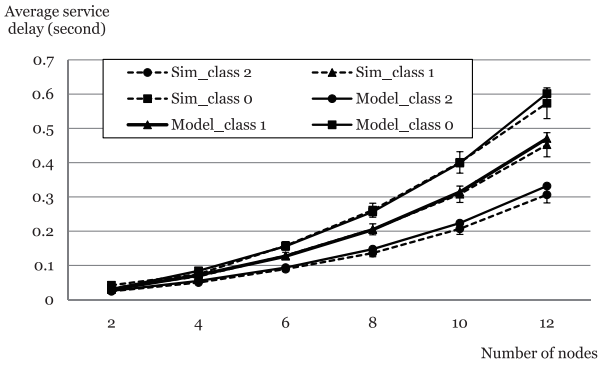

Fig. 7. Comparison of the delay model and simulation service delay results.

classes 0 and 1 approaches a constant as the channel starts to be saturated when λ_g exceeds 55 frames per second.

Figs. 7 and 8 evaluate the precision of our delay and throughput models by contrasting their results to those of the simulation ones. At first, Fig. 7 verifies the accuracy of our service delay model by comparing three pairs of curves when macMaxBE for classes 0, 1, and 2 are set to 8, 6, and 5, respectively. The comparison confirmed that the analytical service delay model is very accurate since the service delay of each class from the analytical model is almost overlapped with those of the same class from simulations. The differences lay in the range of 7.6%.

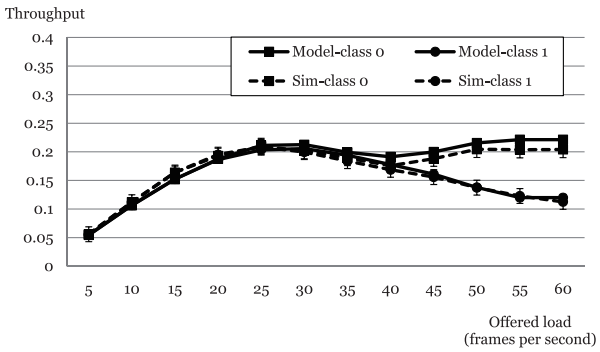

Fig. 8. Comparison of the model and simulation throughput results.

Fig. 8 measures the accuracy of our throughput model by comparing it with simulations under the same conditions as those shown in Fig. 7. The coincidence demonstrates that the throughput model is also precise enough to predict the performance of the multi-queue system. The differences are confined to a range of 7% at maximum.

V. CONCLUSIONS

This paper proposes a multi-queue system to improve QoS support of IEEE 802.15.4 for employment in health-care systems and build its analytical model. It further enhances the accuracy of IEEE 802.15.4 analytical models by including deferment behaviors and transmission retries techniques. The analysis and simulation results predict that the multi-queue system can deliver urgent medical data of higher priority classes rapidly without sacrificing the delays of lower priority classes. In addition, the model proves that the deferment and transmission retries should be accounted for precise forecasts of average delays.

For future research, we will study the effect of burst traffic on the delay and throughput since data traffic from health-care systems is anticipated to come in bursts. Finally, we plan to verify the performance estimated from our model by implementing the multi-queue algorithm in real IEEE 802.15.4 networks.

APPENDIX

In the following appendix, we investigate the impacts of the three operational parameters macMinBE, macMaxBE, and macMaxCSMABackoffs on the average delay. Remember that they are the key factors deciding the priorities of different classes. Table 2 summarizes the various values of parameters for analyses. Each column presents three assigned values of the three parameters for three priority queues. Note that the column labeled with S0 contains the default values of the standard IEEE 802.15.4.

First, for Fig. 9, which corresponds to case S1, macMinBE is set to 3, 2, and 1 for classes 0, 1, and 2, respectively. The graphs illustrate that all of the queues perform worse than the standard. The reason is that the probability of collisions increases due to the shorter backoff window.

Fig. 10 shows the delays when the parameters are set as in case S2. Despite the extended backoff delay, class 0 shows slightly longer delays when the number of nodes is smaller than 10. This is because fewer nodes lead to less frequent collisions, and an extended backoff results in a small increase in overall delay. However, when the number of nodes is 10 or more, the delay of class 0 becomes shorter than that of the standard. This implies that when the network traffic becomes heavy, a longer backoff delay contributes to reducing the collision probability and overall delay. In consequence, by assigning bigger macMaxBE to lower priority queues, we can induce the scheduling to favor higher priority queues.

Fig. 11 compares the performances of S2 and S4. The curves show the impact of macMinBE when the queues take their macMaxBE values as in S2. As in Fig. 11, higher priority classes do not produce improved result. Therefore, reducing macMinBE of higher priority queues for quicker channel access will not improve the performance.

Fig. 12 provides the comparison of the results of S2 and

Table 2. Parameter sets used for each case.

Case		S0	S1	S2	S3	S4	S5
macMinBE	Class 0	3	3	3	3	3	3
	Class 1	3	2	3	3	2	3
	Class 2	3	1	3	3	1	3
macMaxBE	Class 0	5	5	8	5	8	8
	Class 1	5	5	6	5	6	6
	Class 2	5	5	5	5	5	5
macMaxCSMABackoffs	Class 0	4	4	4	6	4	6
	Class 1	4	4	4	5	4	5
	Class 2	4	4	4	4	4	4

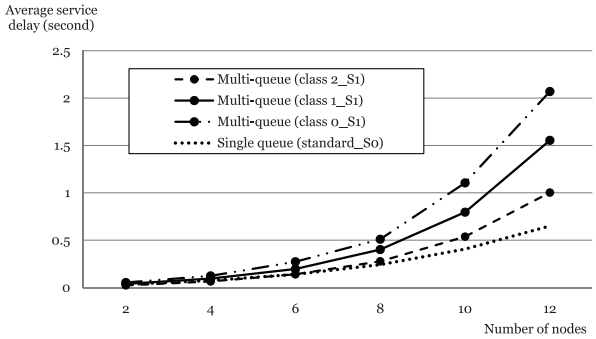

Fig. 9. Effect of macMinBE on delays.

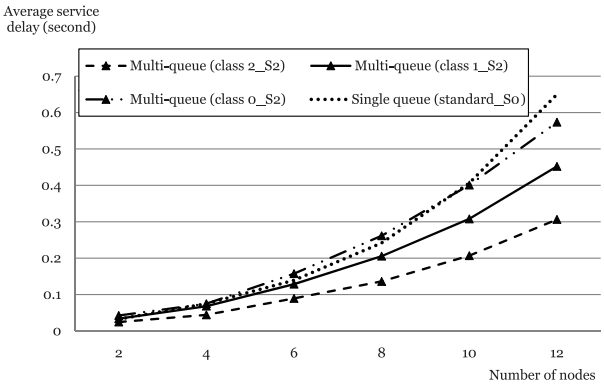

Fig. 10. Effect of macMaxBE on delays.

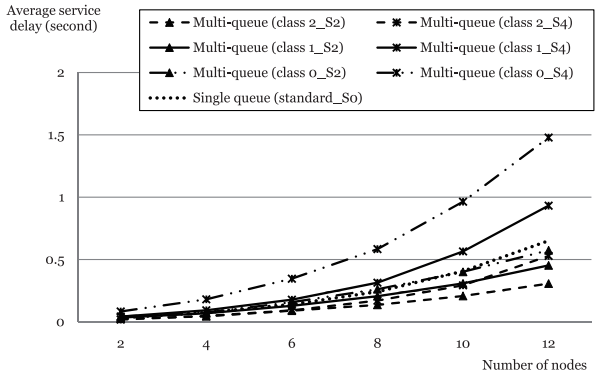

Fig. 11. Combined effect of macMinBE and macMaxBE on delays.

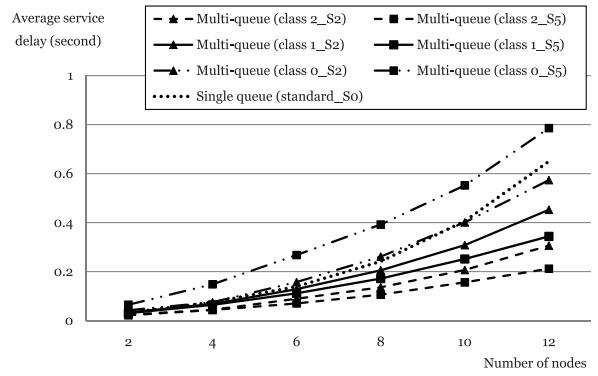

Fig. 12. Combined effect of macMaxBE and macMaxCSMABackoffs on delays.

S5. For S5, the frames of classes 0 and 1 stay longer with expanded backoff delays in the system. This in turn results in that the frames of class 2 have more chances to leave the node. As expected, the curves for class 2 undergo much shorter delays, while class 0 suffers from a delay even longer than that of the standard.

REFERENCES

[1] J. Jung, K. Ha, J. Lee, Y. Kim, and D. Kim, "Wireless body area network in a ubiquitous healthcare system for physiological signal monitoring and health consulting," *Int. J. Signal Process.*, pp. 47–54, 2008.

[2] Y. M. Huang, M. Y. Hsieh, H. C. Chao, S. H. Hung, and J. H. Park, "Pervasive, secure access to a hierarchical sensor-based healthcare monitoring architecture in wireless heterogeneous networks," *IEEE J. Sel. Areas Commun*, vol. 27, no. 4, pp. 400–411, May 2009.

[3] S. Jiang, Y. Cao, S. Iyengar, P. Kuryloski, R. Jafari, Y. Xue, R. Bajcsy, and S. Wicker, "Carenet: An integrated wireless sensor networking environment for remote healthcare," in *Proc. ICST 3rd Int. Conf. Body Area Netw.*, 2008.

[4] R. S. H. Istepanian, E. Jovanov, and Y. T. Zhang, "Guest editorial introduction to the special section on m-health: Beyond seamless mobility and global wireless health-care connectivity," *IEEE Trans. Inf. Technol. Biomed.*, vol. 8, no. 4, pp. 405–414, 2004.

[5] J. Misic and V. B. Misic, "Bridging between IEEE 802.15.4 and IEEE 802.11 networks for multiparameter healthcare sensing," *IEEE J. Sel. Areas Commun.*, vol. 27, no. 4, pp. 435–449, May 2009.

[6] ANSI/IEEE Standard 802.3, Carrier Sense Multiple Access with Collision Detection, 1985.

[7] "IEEE 802.11 WG, part 11: Wireless LAN medium access control (MAC) and physical layer (PHY) specification," IEEE 199pecification, IEEE 1999.

[8] "Wireless medium access control (MAC) and physical layer (PHY) specifications for low-rate wireless personal area networks (LR-WPANs)," IEEE Standard 802.15.4-2003.

[9] "Wireless medium access control (MAC) and physical layer (PHY) specifications for low-rate wireless personal area networks (LR-WPANs)," IEEE Standard 802.15.4-2006.

[10] "Standard for part 15.1: Wireless medium access control (MAC) and physical layer (PHY) specifications for wireless personal area networks (WPAN)," IEEE standard 802.15.1, IEEE, New York, NY, 2002.

[11] "IEEE Std 802.11e-2005 Amendment 8: Medium access control (MAC) quality of service enhancements," 2005.

[12] Z. Chen, C. Lin, H. Wen, and H. Yin, "An analytical model for evaluating IEEE 802.15.4 CSMA/CA protocol in low-rate wireless application," in *Proc. AINAW*, May 2007, pp. 899–904.

[13] J. Misic and V. B. Misic, "Access delay for nodes with finite buffers in IEEE 802.15.4 beacon enabled PAN with uplink transmissions," *Comput. Commun.*, vol. 28, no. 10, pp. 1152–1166, 2005.

[14] J. Misic, V. Misic, and S. Shafi, "Performance of IEEE 802.15.4 beacon enabled PAN with uplink transmissions in non-saturation mode-access delay for finite buffers," in *Proc. BROADNETS*, Oct. 2004, pp. 416–425.

[15] J. Misic and V. B. Misic, *Wireless Personal Area Networks: Performance, Interconnection, and Security with IEEE.802.15.4*. John Wiley & Sons, 2008.

[16] S. Pollin, M. Ergen, S. C. Ergen, B. Bougard, L. van Der Perre, I. Moerman, A. Bahai, P. Varaiya, and F. Catthoor, "Performance analysis of slotted carrier sense IEEE 802.15.4 medium access layer," in *Proc. IEEE GLOBECOM*, Nov. 2006, pp.1–6.

[17] R. K. Patro, M. Raina, V. Ganapathy, M. Shamaiah, and C. Thejaswi, "Analysis and improvement of contention access protocol in IEEE 802.15.4 star network," in *Proc. Mobile Adhoc and Sensor Syst.*, Oct. 2007, pp.1–8.

[18] T. R. Park, T. H. Kim, J. Y. Choi, S. Choi, and W. H. Kwon, "Throughput and energy consumption analysis of IEEE 802.15.4 slotted CSMA/CA," *IEEE Electron. Lett.,* vol. 41, no. 18, pp. 1017–1019, 2005.

[19] S. Y. Lee, Y. S. Shin, J. S. Ahn, and K. W. Lee, "Performance analysis of a non-overlapping binary exponential backoff algorithm over IEEE 802.15.4," in *Proc. ICUT*, Dec. 2009, pp.1–5.

[20] Y. S. Shin, J. S. Ahn, and K. W. Lee, "Analytical performance evaluation of IEEE 802.15.4 with multiple transmission queues for providing QoS under non-saturated condition," in *Proc. APCC*, Oct. 2010.

[21] K. C. Noh, S. Y. Lee, Y. S. Shin, K. W. Lee, and J. S. Ahn, "Performance evaluation of an adaptive congestion avoidance algorithm for IEEE 802.15.4," in *Proc. IEEE CSE*, pp.1–6, 2010.

[22] Y. Xiao, "An analysis for differentiated services in IEEE 802.11 and IEEE 802.11e wireless LANs," in *Proc. IEEE ICDCS,* Mar. 2004, pp. 32–39.

[23] E. J. Kim, M. Kim, S. Youm, S. Choi, and C.-H. Kang, "Priority-based service differentiation scheme for IEEE 802.15.4 sensor networks," *AEUE-Int. J.*, vol. 61, pp. 69–81, 2007.

[24] ns-allinone-2.33.tar.gz. [Online]. Available: http://downloads.sourceforge.net/nsnam/ns-allinone-2.33.tar.gz

Youn-Soon Shin received a B.S. in Computer Science and Statistics in 1999 and an M.S. in Information Communication Engineering in 2002 from Dongguk University in Korea. She is currently working toward her Ph.D. in Information Communication Engineering at Dongguk University. Her interests are wireless sensor networks, IEEE 802.15.4, simulation techniques, and embedded systems.

Kang-Woo Lee received an M.S. and Ph.D. in Electrical Engineering from the University of Southern California in 1991 and 1997, respectively. He also received a B.S. in Electronic Engineering from Yonsei University in 1985. He is currently a Professor at Dongguk University in Korea. His major interests are computer architecture, embedded systems, network computing, and simulation techniques.

Jong-Suk Ahn received a Ph.D. and M.S. in Electrical Engineering from the University of Southern California in 1995 and from the Korean Advanced Institute of Science and Technology in 1985, respectively. He also received a B.S. from Seoul National University in 1983. He was a visiting researcher in ISI/USC for one year in 2001. He was awarded the Gaheon Prize for the best paper in 2003 from the Korean Information Science Society. He is currently a Professor at Dongguk University in Korea. His major interests are sensor networks, dynamic error control and flow control algorithms over wireless Internet, network simulation techniques, IEEE 802.11, and IEEE 802.15.4